Journal of Materials Chemistry C

PAPER

View Article Online
View Journal | View Issue



Cite this: J. Mater. Chem. C, 2018, 6, 4077

# Enhanced luminescence performance of CaO:$Ce^{3+}$,$Li^{+}$,$F^{-}$ phosphor and its phosphor-in-glass based high-power warm LED properties†

Jiankun Deng,[a] Haoran Zhang,[a] Xuejie Zhang,[a] Maxim S. Molokeev,[bcd] Jianbei Qiu,[e] Yingliang Liu,*[a] Bingfu Lei,*[a] Li Ma[f] and Xiaojun Wang[f]

Received 15th February 2018,
Accepted 5th March 2018

DOI: 10.1039/c8tc00813b

rsc.li/materials-c

To obtain white light-emitted diodes (wLEDs) with a low correlated color temperature (CCT) and a high color rendering index (CRI), red-emission is indispensable in their emission spectra. Herein, CaO:$Ce^{3+}$,$Li^{+}$,$F^{-}$ yellow phosphors with more red spectral component have been prepared *via* a high temperature solid-state reaction. As compared to the $F^{-}$ undoped samples, CaO:$Ce^{3+}$,$Li^{+}$,$F^{-}$ phosphor have lower critical doping concentration of $Ce^{3+}$ and show stronger luminescence. At the critical concentration, a quantum efficiency of 66.4% and enhanced thermal and chemical stability were obtained in CaO:$Ce^{3+}$,$Li^{+}$,$F^{-}$. Furthermore, a CaO:$Ce^{3+}$,$Li^{+}$,$F^{-}$-based phosphor-in-glass (PiG) using the red-emitting glass system with the composition of $SiO_2$–$Na_2CO_3$–$Al_2O_3$–CaO:$Eu^{3+}$ as the host material was constructed and used for high-power white LED applications. Such PiG samples with different phosphor doping concentrations can satisfy various light color demands and display higher reliability than the CaO:$Ce^{3+}$,$Li^{+}$,$F^{-}$ phosphor. An optimal PiG-based wLED exhibits color coordinates of (0.3769, 0.3386), a CCT of 3774 K, a CRI of 82.5 and a LE of 73.1 when the mass ratio of phosphor to glass matrix was 7 : 50 in PiG. Moreover, such PiG-based wLED also showed acceptable color stability under different drive currents. All the above results demonstrate that CaO:$Ce^{3+}$,$Li^{+}$,$F^{-}$ can be expected to be a potential alternative yellow phosphor for blue light excited PiG based warm wLEDs, particularly for high-power devices.

## 1. Introduction

Phosphor-converted light emitting diodes (pcLEDs) have become one of the most important tools for solid-state lighting since the development of white LEDs (wLEDs) fabricated using the combination of a InGaN blue LED chip and $Ce^{3+}$-doped yttrium aluminum garnet (YAG:$Ce^{3+}$).[1,2] Nevertheless, some shortcomings, including a high correlated color temperature (CCT) and low color rendering index (CRI), do exist with such outstanding light emitting devices. For the resolution of the abovementioned issues, adding a red spectral component in the emission spectra of wLEDs through supplementing a red phosphor or substitution of YAG:$Ce^{3+}$ by a yellow-emitting phosphor is the most frequently used method.[3,4] Nowadays, owing to the limited availability of red phosphors with suitable spectral properties, alternative yellow-emitting phosphors (*e.g.* YAG:$Ce^{3+}$ compositional derivatives), which are specifically developed for adjusting their luminescence properties to obtain more red emission components, have received more attention.[4] In the evolution of this class of yellow-emitting phosphors, ion substitution is the main approach to achieve these desired objectives.[5–9] The development of other novel yellow-emitting phosphors should be increasingly facilitated for the sake of resource conservation and environmental friendliness.

Calcium oxide (CaO), with the characteristics of abundance, low price and non-toxicity, has been widely applied in different fields, such as ceramics, glass and catalysis.[10–12] Moreover, CaO can be doped with various rare earth ions to obtain a series of phosphor-materials with special properties such as harvesting photoluminescence, electron degradation, thermoluminescence, long persistence and energy transfer.[13–18] Among the CaO-phosphors, $Ce^{3+}$-doped CaO (CaO:$Ce^{3+}$) with simple chemical composition, suitable excitation and emission spectra is a promising yellow-emitting phosphor for blue light excited wLEDs.

[a] Guangdong Provincial Engineering Technology Research Center for Optical Agricultural, College of Materials and Energy, South China Agricultural University, Guangzhou 510642, China. E-mail: tleibf@scau.edu.cn
[b] Laboratory of Crystal Physics, Kirensky Institute of Physics, Federal Research Center KSC SB RAS, Krasnoyarsk 660036, Russia
[c] Department of Physics, Far Eastern State Transport University, Khabarovsk 680021, Russia
[d] Siberian Federal University, Krasnoyarsk, 660041, Russia
[e] Faculty of Materials Science and Engineering, Kunming University of Science and Technology, Kunming, 650093, China
[f] Department of Physics, Georgia Southern University, Statesboro, GA 30460, USA
† Electronic supplementary information (ESI) available. See DOI: 10.1039/c8tc00813b

In addition, the emission spectrum of CaO:$Ce^{3+}$ possesses more red spectral components than the commercialized YAG:$Ce^{3+}$, making it more appropriate for warm-wLEDs. However, the low efficient light conversion and weak chemical stability of CaO:$Ce^{3+}$ are the main factors that restrict its feasibility to replace YAG:$Ce^{3+}$. To date, some studies have been reported on solving these problems. For example, Hao *et al.* proposed that alkali metal ion ($Li^+$ or $Na^+$) co-doping can effectively increase the photoluminescence intensity in CaO:$Ce^{3+}$.[19,20] Lehmann found that coating a layer of $CaF_2$ on the surface of CaO:$Ce^{3+}$ particles can slow down the reaction between CaO:$Ce^{3+}$ and atmospheric moisture.[13] In general, research on CaO:$Ce^{3+}$ phosphor is still relatively scarce and needs more investment.

In recent years, a new class of luminescent material, namely, phosphor-in-glass (PiG) has been developed to use in the application of color converters that are required to have high performance.[21] In the preparation process of such PiG-materials, low-melting inorganic glass powder is chosen to be the encapsulant and translated into the glass matrix used to coat the traditional phosphors at a low sintering temperature, which makes PiG retain the advantages of glass, such as high thermal conductivity, excellent chemical stability and good plasticity. Because of the glass-like properties, PiG can resist the heat generated from the high-power LED chip or laser excitation in order to keep from altering the yellowing of its body-color and resist the influences of its environment as compared to the color converters fabricated using silicone as the encapsulant. A few previous studies have also confirmed the importance of PiG for high-power lighting devices. In 2012, Chung *et al.*[22] pioneered the use of YAG:$Ce^{3+}$-PiG in high-power wLEDs. Subsequently, YAG:$Ce^{3+}$-PiG and other phosphor-PiGs as color converters have undergone great development.[23–27] In particular, researchers have recently applied PiG in laser illumination.[28,29] Thus it can be seen that PiG technology can enable phosphors to be suitable for high-power lighting devices. In addition, as a robust encapsulant, the glass matrix of PiG can emit red light *via* trivalent ion (*e.g.* $Eu^{3+}$,$Pr^{3+}$) doping, thus improving the optical properties of their corresponding white light devices.[30–32]

On the basis of the abovementioned considerations, we believe that PiG technology will be a good accompaniment to CaO:$Ce^{3+}$ phosphors in the respect to the color converters. In this research, $Ce^{3+}$,$Li^+$,$F^-$ triply-doped CaO (CaO:$Ce^{3+}$,$Li^+$,$F^-$) phosphor with enhanced luminescence and thermal stability was successfully prepared through a high-temperature solid phase method. The effects of $F^-$ co-doping on the various properties of CaO:$Ce^{3+}$,$Li^+$ are discussed in detail. A series of robust multi-color CaO:$Ce^{3+}$,$Li^+$,$F^-$-PiGs were synthesized by combining CaO:$Ce^{3+}$,$Li^+$,$F^-$ and the red-emitting glass system with the composition of $SiO_2$–$Na_2CO_3$–$Al_2O_3$–CaO:$Eu^{3+}$, demonstrating great potential for high-power warm wLEDs.

# 2. Experimental method

## 2.1 Preparation

The synthesis process used to prepare CaO:$x$$Ce^{3+}$,$x$$Li^+$,4$x$$F^-$ ($x$ = 0.0004, 0.0006, 0.0008, 0.0012, 0.003, 0.005, 0.007, 0.009, 0.011 and 0.013) *via* a high temperature solid-state reaction was as follows. Stoichiometric amounts of the raw materials CaO, CeF and LiF were mixed thoroughly and then, the mixture was heated in a tube furnace at 5 °C $min^{-1}$ to 1400 °C for 6 h under reducing atmosphere (5% $H_2$ + 95% $N_2$). The as-obtained samples were cooled naturally to room temperature in the furnace and then ground into powder for the subsequent tests. The $F^-$ undoped samples of CaO:$y$$Ce^{3+}$,$y$$Li^+$, ($y$ = 0.003, 0.005, 0.0007, 0.009, 0.011 and 0.013) using $CeO_2$ and $Li_2CO_3$ as the cerium and lithium sources, respectively, were chosen as the references and prepared under the same conditions. In addition, CaO:$x$$Ce^{3+}$,$x$$Li^+$,4$x$$F^-$ ($x$ = 0.0006) and CaO:$y$$Ce^{3+}$,$y$$Li^+$ ($y$ = 0.007), which are representative samples, were denoted as COCLF-6 and COCL-7, respectively, in the subsequent discussions for concise expression.

PiG samples with different mass ratios of the phosphor to glass matrix (3 : 50, 5 : 50, 3 : 50 and 9 : 50) were initially prepared using the mixtures of COCLF-6 and the precursor glass frit with the composition of $SiO_2$–$Na_2CO_3$–$Al_2O_3$–CaO:$Eu^{3+}$, which was developed in our previous study.[32] Then, the mixtures were compressed into cylinders and sintered at 5 °C $min^{-1}$ to 680 °C for 0.5 h under air atmosphere. The as-obtained PiG plates were cut into the desired size ($\phi$ 10 mm disk with thickness of 0.5 mm) and then optically polished. The corresponding PiG-based wLEDs were fabricated using a combination of the PiG samples and 460 nm high-power blue chip.

## 2.2 Characterization

The photoluminescence excitation (PLE) and photoluminescence (PL) spectra were recorded on a F-7000 Hitachi fluorescence spectrofluorometer. The decay curves were recorded using the kinetic mode of a FSP920 time-resolved and steady state fluorescence spectrometer (Edinburgh Instruments, England) equipped with a 150 W nF900 flash lamp as the light source. The structure and phase purity of the samples were analyzed using powder X-ray diffraction (XRD) on a Rigaku Ultima-IV X-ray diffractometer with Cu Kα radiation ($\lambda$ = 0.15406) at 40 kV and 40 mA. Rietveld analysis for the powder diffraction data of the samples was performed using the TOPAS 4.2 system. The X-ray photoelectron spectroscopy (XPS) patterns were recorded by employing a Kratos AXIS Ultra DLD X-ray photoelectron spectrometer using a monochromatic Al Kα X-ray source. The morphological observations were obtained through transmission electron microscopy (TEM) and high-resolution transmission electron microscopy (HRTEM) using a JEOL-2010 electron microscope equipped with an energy-dispersive X-ray spectroscopy (EDS) system. The distributions of the phosphor and PiG samples were investigated using an ultra-high resolution field-emission scanning electron microscope (FEI, Nova NanoSEM 430) and a confocal laser scanning microscope (LSM 710, Zeiss), equipped with a 458 nm laser for excitation, respectively. The quantum efficiency (QE) was measured by QY2000 (Tianjin Orient-KOJI Instrument, China). The temperature-dependent PL spectra were measured using an F-4600 fluorescence spectrophotometer combined with a heating apparatus (Oxford Instruments). The electroluminescence (EL) of the PiG-based wLEDs and their corresponding parameters were

 

measured on a FSP920 under 9 V operating voltage with various driving currents. The chemical stability of the samples was examined by exposing them to ambient atmosphere for the time period of 10 days.

## 3. Results and discussion

Based on its suitable photoluminescence properties, the CaO:$Ce^{3+}$,$Li^{+}$,$F^{-}$ phosphor is a good candidate for use in 460 nm blue light excited wLEDs. The PLE and PL spectra of COCLF-6 are shown in Fig. 1A, displaying the excitation band located at 458 nm and the emission band at around 560 nm. The former band originating from the $4f^1 \rightarrow 5d^1$ transition of $Ce^{3+}$ involves no ultraviolet excitation wavelength, which can eliminate the effect of the absorption of the glass host when the CaO:$Ce^{3+}$,$Li^{+}$,$F^{-}$ phosphor is applied in PiG-materials. The emission broadband is asymmetric and can be fitted into two Gaussian bands centered at 552 nm (P1, $T_{2g} \rightarrow {}^2F_{5/2}$) and 620 nm (P2, $T_{2g} \rightarrow {}^2F_{7/2}$). The energy difference between these two Gaussian bands is 1987 $cm^{-1}$, which is in accordance with the energy gap between $^2F_{5/2}$ and $^2F_{7/2}$. Moreover, in comparison with that of YAG:$Ce^{3+}$, the PL spectrum of COCLF-6 has higher red spectral component, which is required for the fabrication of wLEDs with high CRI and low CCT (Fig. S1, ESI†). Photographs of the COCLF-6 phosphor in daylight, under 365 nm UV light and under 460 nm blue light excitation are also illustrated in the inset of Fig. 1A. As shown in Fig. 1B, the PL intensity reaches a maximum in CaO:$Ce^{3+}$,$Li^{+}$,$F^{-}$ at a doping concentration of $x$ = 0.0006, while the critical concentration of $y$ = 0.007 is obtained in CaO:$Ce^{3+}$,$Li^{+}$. Remarkably, the variance between the critical concentrations in these phosphors is about 10 times and a higher intensity was found in CaO:$Ce^{3+}$,$Li^{+}$,$F^{-}$, indicating that $F^{-}$ ion co-doping exerts an important influence on the state of the activator ion ($Ce^{3+}$) in the CaO host. As shown in the insets of Fig. 1B, the $F^{-}$ doped samples have deeper body-color than the undoped samples at the same doping concentration ($x$ = 0.003–0.013) of $Ce^{3+}$, further confirming the above viewpoint. In order to establish the energy transfer mechanism accounting for the concentration quenching, the critical distance ($R_c$) can be calculated using the following formula[18,33]

$$R_c = 2\left(\frac{3V}{4\pi x_c N}\right)^{1/3} \quad (1)$$

where $x_c$ represents the critical doping concentration of $Ce^{3+}$, while $V$ and $N$ are the unit cell volume of the altered CaO host and the number of unit cell sites occupied by $Ce^{3+}$, respectively. According to the results of the Rietveld structural refinements (Table 1), the $R_c$ values for COCLF-6 and COCL-7 are 44.6 Å and 19.6 Å, respectively. Thus, the type of concentration quenching mechanism in both materials is the multipole–multipole interaction because of the inconsistency with the other mechanisms, including the exchange interaction ($R_c \approx 4$ Å) and radiation reabsorption (limited overlap between PLE and PL spectra). Moreover, multipole interactions can be subdivided into several types using the Dexter theory and identified using the following equation:[34]

$$I/x = k[1 + \beta(x)^{\theta/3}]^{-1} \quad (2)$$

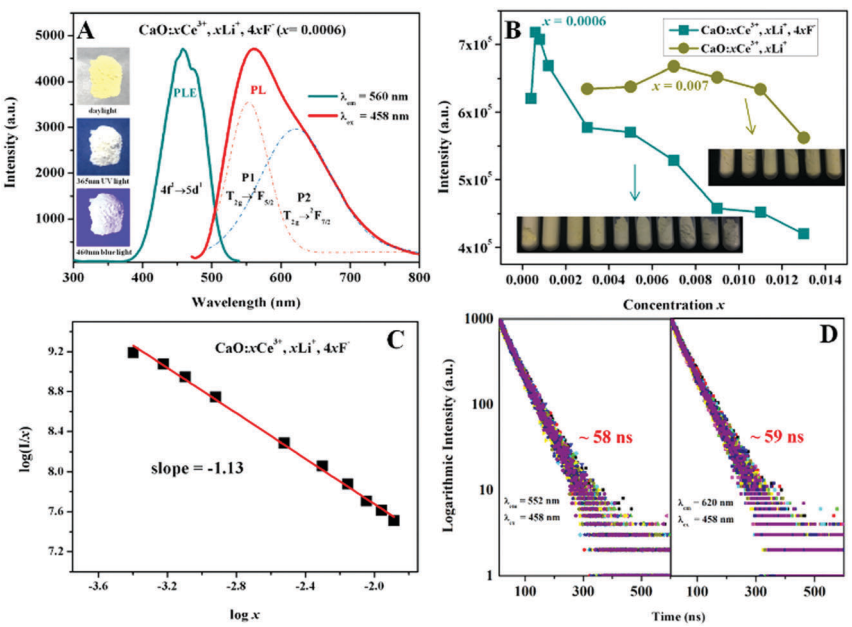


Fig. 1 (A) PLE and PL spectra of the COCLF-6 phosphor. The insets show photographs of the COCLF-6 phosphor in daylight, under 365 nm UV light and under 460 nm blue light excitation. (B) Dependence of the emission intensity *versus* $x$ in CaO:$x$$Ce^{3+}$,$x$$Li^{+}$,4$x$$F^{-}$ (bluish green line) and CaO:$y$$Ce^{3+}$,$y$$Li^{+}$ (yellow line) excited at 458 nm. Insets are photographs of the corresponding samples with various doping concentrations $x$ in daylight. (C) log($I$/$x$) as a function of the doping concentration $x$ in CaO:$x$$Ce^{3+}$,$x$$Li^{+}$,4$x$$F^{-}$. (D) Decay curves of the $T_{2g} \rightarrow {}^2F_{5/2}$ (left) and $T_{2g} \rightarrow {}^2F_{7/2}$ (right) transitions observed for the different doping concentrations $x$ (0.0004–0.013) in CaO:$x$$Ce^{3+}$,$x$$Li^{+}$,4$x$$F^{-}$.

Table 1 Rietveld structure refinement data obtained for COCLF-6 and COCL-7

| Sample | Phase | Space group | Cell parameters (Å) | Cell volume (Å$^3$) | $R_B$ (%) | $R_{wp}$ (%) | $R_p$ (%) | $\chi^2$ | Content weight (%) |
|---|---|---|---|---|---|---|---|---|---|
| COCLF-6 | CaO | $Fm\bar{3}m$ | $a = b = c = 4.8087$ (5) | $V = 111.20$ (3) | 2.72 | 9.19 | 6.27 | 1.42 | 93.8 (7) |
| | $Ca(OH)_2$ | $P\bar{3}m1$ | $a = b = 3.577$ (6), $c = 4.918$ (9) | $V = 54.5$ (2) | 2.31 | | | | 5.6 (7) |
| | $CeO_2$ | $Fm\bar{3}m$ | $a = b = c = 5.3214$ (2) | $V = 150.69$ (1) | 8.08 | | | | 0.6 (2) |
| COCL-7 | CaO | $Fm\bar{3}m$ | $a = b = c = 4.8085$ (4) | $V = 111.19(3)$ | 7.17 | 11.72 | 8.62 | 1.70 | 90.5 (9) |
| | $Ca(OH)_2$ | $P\bar{3}m1$ | $a = b = 3.589$ (3), $c = 4.918$ (5) | $V = 54.9$ (1) | 5.30 | | | | 7.9 (9) |
| | $CeO_2$ | $Fm\bar{3}m$ | $a = b = c = 5.4156$ (2) | $V = 158.84$ (2) | 5.84 | | | | 1.6 (1) |

where $x$ and $I$ represent the concentration of $Ce^{3+}$ activator and the corresponding PL intensity, respectively; $k$ and $\beta$ are the constants for the individual interactions in the given matrix; $\theta$ can be assigned various values such as 3, 6, 8 or 10, which indicate the energy migration among nearest neighbor or next nearest neighbor activators, dipole–dipole interaction, dipole–quadrupole interaction, or quadrupole–quadrupole interaction, respectively. For the calculation of $\theta$, the slope ($\theta$/3) should be first obtained from the relationship of $\log I/x$ with $\log x$ by simplifying eqn (2). Therefore, the slopes of the fitting lines are −1.13 and −1.05 (Fig. 1C and Fig. S2, ESI†), indicating that the concentration quenching behaviour occurring in the $F^-$ doped and undoped samples are owing to the energy migration among nearest neighbor or next nearest neighbor activators. In other words, $F^-$ doping does not affect the concentration quenching mechanism of CaO:$Ce^{3+}$,$Li^+$, but lowers its critical quenching concentration, the reason of which may be ascribed to the fact that the environment in which the anion ($O^{2-}$) is located is changed by the incorporation of $F^-$, while the environment in which the cation ($Ca^{2+}$) is located does not change. As shown in Fig. 1D, the PL decay curves observed for the transitions $T_{2g} \rightarrow {}^2F_{5/2}$ and $T_{2g} \rightarrow {}^2F_{7/2}$ in CaO:$x$$Ce^{3+}$,$x$$Li^+$,4$x$$F^-$ ($x$ = 0.0004–0.0013) excited at 458 nm and monitored at 552 nm and 620 nm, respectively were fitted with a single-exponential function and their lifetimes were calculated according to the following equation:

$$I = A\exp\left(\frac{-t}{\tau}\right) \quad (3)$$

where $I$ represents the PL intensities at time $t$; $A$ and $\tau$ are the constant and the lifetime, respectively. The values of the lifetimes for the two transitions are ~58 ns and ~59 ns, which remains almost the same when the $Ce^{3+}$ concentration is changed. The above results indicate that even though the energy migration among nearest neighbor or next nearest neighbor $Ce^{3+}$ exists, they have very limited influence on the concentration quenching behavior of CaO:$Ce^{3+}$,$Li^+$,$F^-$. In fact, the PL intensity of CaO:$Ce^{3+}$,$Li^+$,$F^-$ with different doping concentrations should depend on the number of $Ce^{3+}$ absorbing excitation photons.[19,20]

To further understand the role that $F^-$ doping plays in CaO:$Ce^{3+}$,$Li^+$ to cause these unique optical properties, the structural analysis of CaO:$Ce^{3+}$,$Li^+$,$F^-$ and CaO:$Ce^{3+}$,$Li^+$ were studied. The X-ray diffraction (XRD) patterns of CaO:$x$$Ce^{3+}$,$x$$Li^+$,4$x$$F^-$ ($x$ = 0.0004–0.0013) are given in Fig. 2A, which shows that all the distinct characteristic diffraction peaks coincide with those of a standard CaO sample (PDF #37-1497), except the one centered at $\theta = 28.5^\circ$, which is arises due to the $CeO_2$ impurity (red rectangle). A similar situation also exists for CaO:$y$$Ce^{3+}$,$y$$Li^+$ ($y$ = 0.003–0.013) as shown in Fig. 2B. Upon the replacement of $Ca^{2+}$ ($r$ = 1 Å) with $Ce^{3+}$ ($r$ = 1.02 Å) and $Li^+$ ($r$ = 0.76 Å), the diffraction peaks of the CaO host should shift to a higher angle because of the radius diversity of the ions ($2r_{Ca^{2+}} > r_{Ce^{3+}} + r_{Li^+}$). However, this phenomenon does not appear in CaO:$Ce^{3+}$,$Li^+$,$F^-$ and CaO:$Ce^{3+}$,$Li^+$ (Fig. 2C). More structural information can be obtained from the Rietveld refinement analysis of COCLF-6 and COCL-7 performed using TOPAS 4.2.[35] Almost all of the peaks are indexed to the CaO,$Ca(OH)_2$ and $CeO_2$ phases.[36–38] Therefore, these structures were taken as a starting model for Rietveld refinement. The refinements for both samples are stable and give low $R$-factors (Fig. 3 and Table 1). It is worth noting that in addition to CaO and $CeO_2$, the $Ca(OH)_2$ impurity was detected at

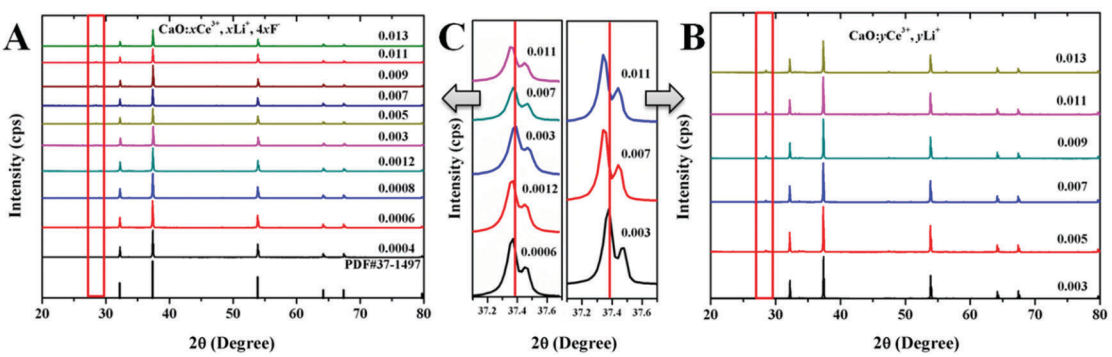


Fig. 2 XRD patterns of (A) CaO:$x$$Ce^{3+}$,$x$$Li^+$,4$x$$F^-$ ($x$ = 0.0004–0.013), standard cubic for CaO (PDF #37-1497) and (B) CaO:$y$$Ce^{3+}$,$y$$Li^+$ ($y$ = 0.003–0.013). (C) The enlarged XRD patterns of the corresponding samples from 37.0° to 37.8°.

 

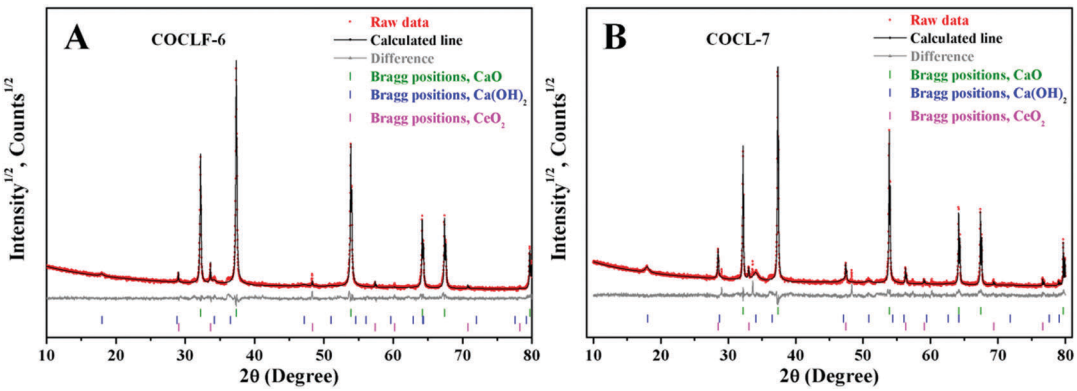


Fig. 3 Rietveld refinement analysis of (A) COCLF-6 and (B) COCL-7. Raw data, calculated patterns and the difference between them are presented using red dots, black lines and grey lines, respectively, while the Bragg positions of CaO, $Ca(OH)_2$ and $CeO_2$ are marked with green, blue and pink vertical lines, respectively.

the same time and the content of $Ca(OH)_2$ in COCLF-6 was lower than that in COCL-7, implying that a small amount of $F^-$ doping is advantageous to the protection of CaO from water infiltration.[13] Moreover, the cell volume of both samples are nearly identical and become larger when compared to the starting model, which is in good agreement with the XRD results shown in Fig. 2C. Based on the above experimental evidence, the doping mode of the Ce ($Ce^{3+}$ and $Ce^{4+}$) and $Li^+$ ions in CaO is illustrated in Fig. 4A. Inevitably, Ce ions in different states of valence were maintained during the doping process as indicated by the XPS spectra of Ce 3d (Fig. S3, ESI†).[39] According to the previous study reported by Liu *et al.*,[40] it can be deduced that some $Ca^{2+}$ sites in the CaO host lattice are occupied by $Ce^{3+}$, while the other sites are accommodated by $Ce^{4+}$. The co-dopant of $Li^+$ was introduced into the interstitial sites as the donor, providing electrons for $Ce^{4+}$. Thus, not only the cell volume, but also the concentration of activator $Ce^{3+}$ increased, leading to the enhanced PL intensity of CaO:$Ce^{3+}$,$Li^+$. In addition, the cell volume of COCLF-6 ought to be smaller than COCL-7 owing to the lower doping concentration of $Ce^{3+}$ and $Li^+$ as well as the replacement of $O^{2-}$ by $F^-$ ($r_{O^{2-}} > r_{F^-}$). However, as a matter of fact, the cell volume of the former equals or even exceeds that of the latter. This may be because $F^-$ was successfully doped into the CaO host lattice as indicated by the absence of the phase related to $F^-$ in the corresponding XRD patterns. In addition, two $F^-$ ions, instead of one, were substituted per $O^{2-}$ ion, thus maintaining the charge balance, so that COCLF-6 has a larger cell volume (Fig. 4B). As for the increase in the PL intensity of COCLF-6, as compared to COCL-7, we assume that the introduction of $F^-$ will reduce the distance between the $Ce^{3+}$ activator and result in the decrease in the critical quenching concentration of $Ce^{3+}$, thus increasing the PL intensity. Nevertheless, the content of the $Ca(OH)_2$ impurity in COCLF-6 was also reduced, which was beneficial for the improvement in PL performance.[20] The comprehensive influence of these two factors mentioned above determines the optical properties of COCLF-6.

The microstructure of COCLF-6 is displayed in Fig. 5. The TEM image shows that a single particle of the measured sample has an irregular shape with the particle size of $\sim$3 μm (Fig. 5A). The elements Ca, O, Ce and F are distributed homogeneously in the single particle of COCLF-6, further proving that the dopants, $F^-$ in particular, have been incorporated into the CaO host lattice (Fig. 5B–E). As shown in Fig. 5F and G, the spacing of the lattice fringe in the HRTEM image is 2.73 Å and the characteristic planes of CaO can be well indexed to the concentric ring patterns in the selected area electron diffraction

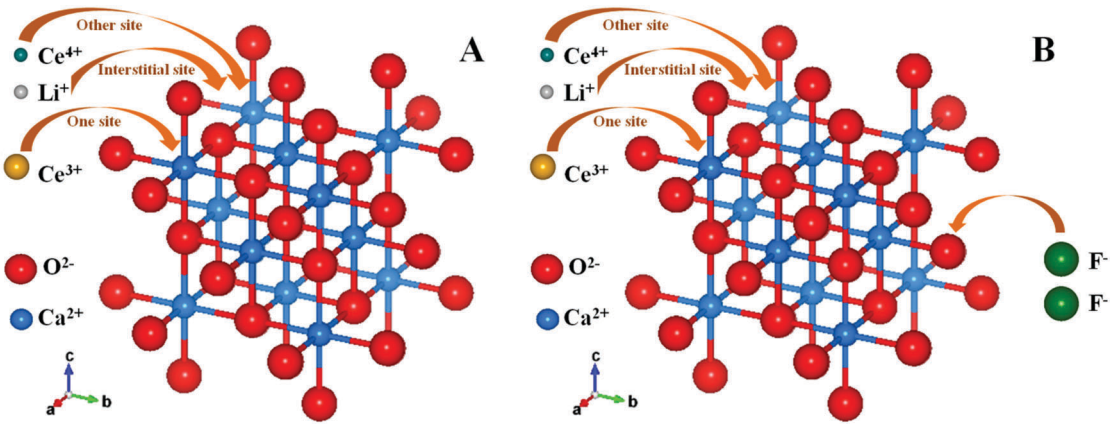


Fig. 4 Schematic illustrations of the doping of CaO with different ions, including (A) $Ce^{3+}$,$Ce^{4+}$,$Li^+$ and (B) $F^-$.

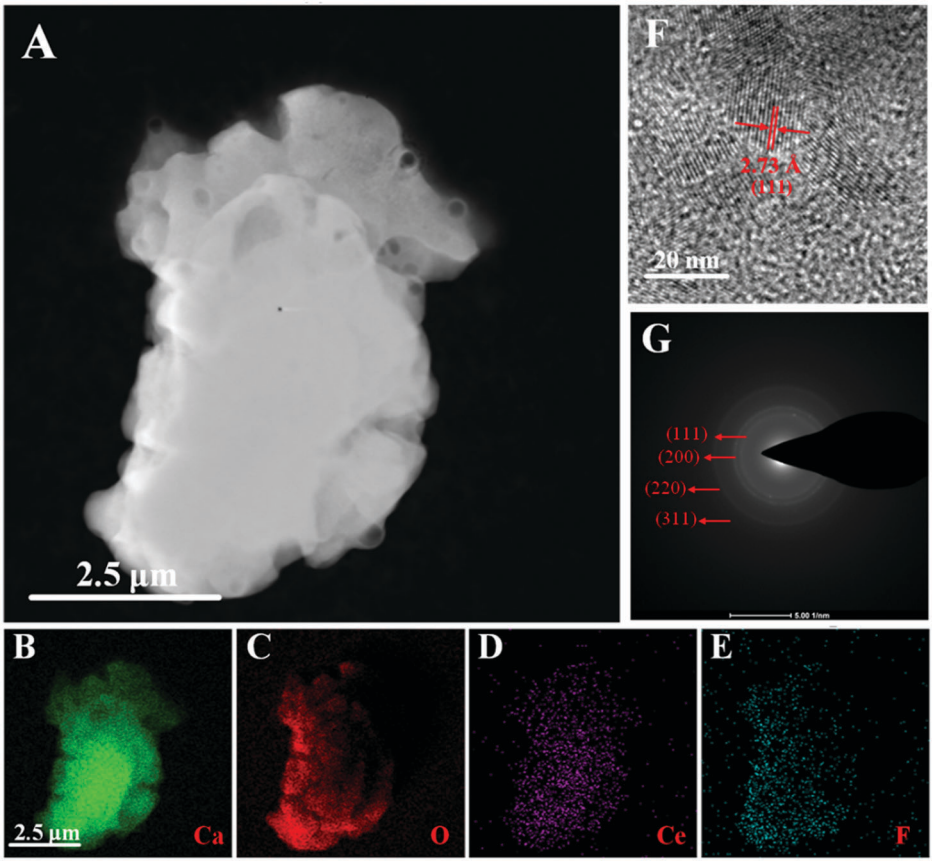


Fig. 5 (A) TEM image of a single particle of COCLF-6 and (B–E) corresponding elemental mappings of Ca, O, Ce and F. (F) HRTEM image and (G) SAED pattern of COCLF-6.

(SAED) pattern, both of which confirm that the CaO phase is dominant in the specimen.[41] Additionally, the scanning electron microscopy (SEM) image of COCLF-6 is presented in Fig. S4 (ESI†), showing slight agglomeration in the as-synthesized phosphor powders.

In particular, a detailed comparison between COCLF-6 and COCL-7 was carried out and the advantage of the former over the latter was obtained. First, the QEs of the materials were measured and described using following equation:

$$\eta_{QE} = \frac{\int L_s}{\int E_r - \int E_s} \quad (4)$$

where $L_s$ presents the emission spectrum of the sample under excitation outside the integrated sphere, while $E_r$ and $E_s$ are the emission spectra obtained inside the integrated sphere under excitation without the sample and with the sample under excitation, respectively. After the calculation, the QE of COCLF-6 was 66.4% when excited at the wavelength of 458 nm. Under the same conditions, the QE of COCL-7, which is 40.1%, was more negative, declining by 66%. We may draw the conclusion that the $F^-$ doped sample with enhanced luminescence was more conducive as the color converter. Second, an improvement in the thermal stability was found in COCLF-6 as compared to COCL-7 as shown in the temperature-dependent PL spectra ranging from 30 to 300 °C at intervals of 30 °C (Fig. 6A). With an increase in temperature, the PL intensities of the both samples show a descending trend owing to the aggravation of non-radiative transfer.[42] However, the PL intensities of the $F^-$ doped and undoped samples can be separately maintained at 88.9% and 77.6%, respectively at a temperature of 150 °C, which greatly caters for the desired high-power LED applications. Furthermore, the parameter of the activation energy ($E_a$) can give more information about thermal quenching behavior of the samples and can be estimated using following equation:[42]

$$I(T) = \frac{I_0}{1 + A\exp\left(-\frac{E_a}{kT}\right)} \quad (5)$$

where $I_0$ is the PL intensity at the initial temperature (30 °C), while $I(T)$ is the PL intensity at the measured temperature; $A$ and $k$ are the constant and the Boltzmann constant, respectively. As shown in the inset of Fig. 6, COCLF-6 has larger $E_a$ than COCL-7, which indicates that the excitation process of the electrons of $Ce^{3+}$ becomes more effective in the $F^-$ doped sample, which has lower thermal energy.[43] As CaO easily reacts with water, it is unstable when exposed to atmospheric moisture. Thus, preventing the CaO phosphor from transforming into $Ca(OH)_2$ is crucial. Fig. 6B shows the time-dependent PL intensity of COCLF-6 and COCL-7 when exposed to air. After 10 days of exposure to air, the PL intensity of COCLF-6 remained at 29.4%,

 

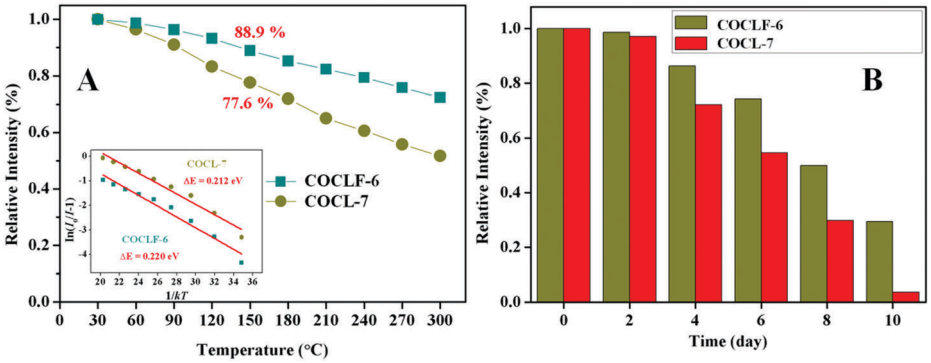


Fig. 6 (A) Temperature-dependent PL intensity of COCLF-6 and COCL-7. Corresponding $\ln(I_0/I - 1)$ as a function of $1/kT$ and $\Delta E$ are shown in the inset. (B) Relative intensity as a function of time in COCLF-6 and COCL-7 when exposed to air.

while that of COCL-7 was 3.7%. Furthermore, $F^-$ doping can effectively help in improving the chemical stability of the CaO phosphor.

For application in high-power wLED devices, the color converter composed of the encapsulant and phosphor should have outstanding thermal stability. Clearly, PiG technology that involves glass material as the encapsulant can be well-applicable for the preparation method of the required color converter. To this end, the COCLF-6 phosphor was incorporated into a red-emitting glass system with the composition of $SiO_2$–$Na_2CO_3$–$Al_2O_3$–CaO:$Eu^{3+}$ to form multi-color PiG with different mass ratios of phosphor to glass matrix ranging from 3 : 50 to 9 : 50. Fig. 7A shows the XRD patterns of the host glass and COCLF-6-based PiG (mass ratio = 7 : 50). One broad band representing amorphous nature was found for the host glass, while the PiG displays an amorphous hump with other diffraction peaks belonging to the CaO phase. The XRD analysis results indicate that there was no phase transition occurring in the embedded phosphor during the PiG preparation process. The distribution of the phosphor particles inside the PiG can be observed using a confocal laser scanning microscope (CLSM) with 458 nm excitation wavelength; the upper surface LSM image of COCLF-6-based PiG (mass ratio = 7 : 50) is shown in Fig. 7B. The yellow highlights with some agglomerations are almost filled over the entire area, demonstrating that COCLF-6 can be distributed homogeneously in the glass matrix. The agglomeration phenomenon can be eliminated by applying better pulverization technology in the future.

The PLE spectra of COCLF-6 and the host glass are displayed in Fig. 8A. The f–f transition of $Eu^{3+}$ in the host glass leads to characteristic excitation peaks, particularly the peak located at round 460 nm. The excitation peak of the host glass overlaps well with that of the COCLF-6 phosphor, which can give the corresponding PiG a double color-emitting property when excited at the same wavelength. As expected, the emission peaks of the host glass originate from the $^5D_0 \rightarrow {}^7F_J$ ($J$ = 0–4) transition, while that of the phosphor, under 458 nm excitation, can be observed in the PL spectra of the COCLF-6-based PiG (mass ratio = 7 : 50) (Fig. 8B). With the addition of the red-emitting $Eu^{3+}$ provided by the host glass, the PiG sample as a color converter can offer more red spectral components in the emission spectra when it is used for warm wLED applications.[25] Fig. 8C shows the PL spectra of the PiG samples with different mass ratios of phosphor to glass matrix ranging from 3 : 50 to 9 : 50. The $Ce^{3+}$: 5d → 4f emission intensity of PiG increases upon increasing the phosphor doping concentration, satisfying various light color demands. As shown in Fig. S5A and B (ESI†), the thermal and chemical stability of the COCLF-6-based PiG significantly improved as compared to that of COCLF-6 phosphor. Impressively, the PL intensity of the PiG sample remains at about 90.4% after 10 days exposure to air, signifying that the COCLF-6 phosphor can be protected through PiG technology and has become more satisfactory for high-power wLEDs.

PiG-based wLEDs with different mass ratios of phosphor to glass matrix ranging from 3 : 50 to 9 : 50 were fabricated by a

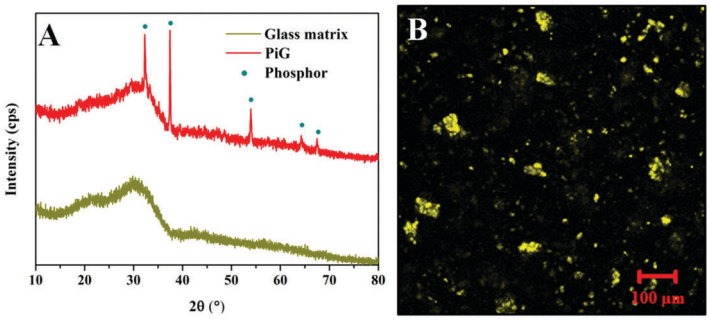


Fig. 7 (A) XRD patterns of the host glass and COCLF-6-based PiG (mass ratio = 7 : 50). (B) The upper surface LSM image of COCLF-6-based PiG (mass ratio = 7 : 50).

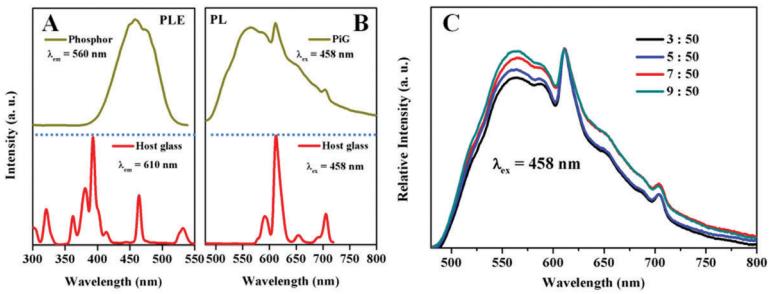


Fig. 8 (A) PLE spectra of the COCLF-6 and host glass. (B) PL spectra of the COCLF-6-based PiG (mass ratio = 7 : 50) and host glass. (C) PL spectra of the PiG with different mass ratios of phosphor to glass matrix ranging from 3 : 50 to 9 : 50.

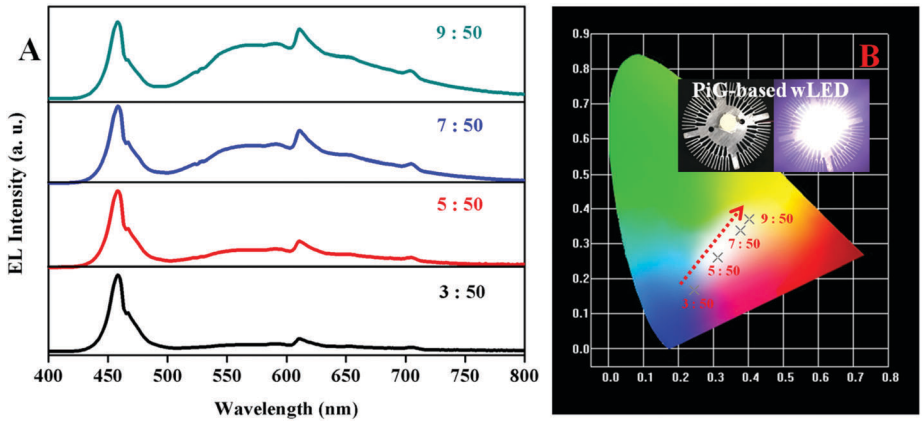


Fig. 9 (A) EL spectra and (B) CIE color coordinates of the PiG-based wLEDs with different mass ratios of phosphor to glass matrix ranging from 3 : 50 to 9 : 50 using a 50 mA operating current. The insets of (B) show the images of the PiG (mass ratio = 7 : 50)-based wLEDs out of operation and in operation.

combination of the PiG samples and a 460 nm high-power blue chip, and the EL spectra recorded with 50 mA operating current are displayed in Fig. 9A. The emissive component of PiG increases with an increase in the mass ratio of phosphor to glass matrix. The Commission Internationale de L'Eclairage (CIE) color coordinates and the corresponding EL parameters are shown in Fig. 9B and Table 2, respectively. The emitting color of the as-fabricated PiG-based wLEDs can be modified from blue-white to cool white and subsequently to warm white, and the coordinates of these wLEDs change from (0.2439, 0.1686) to (0.4036, 0.3707). Apart from the blue-white wLED, the other wLEDs show CCT ranging from 7487 to 3364 K and LE (luminous efficacy) decreasing from 78.6 to 68.4, while the optimal CRI value of 82.5 is achieved in the wLED, whose mass ratio was 7 : 50. The images of the PiG (mass ratio = 7 : 50)-based wLEDs out of operation and in operation are also supplied in the inset of Fig. 9B. The abovementioned results demonstrate that the as-obtained PiG-based wLEDs, particularly that with high CRI, can be better applied in indoor illumination.

Table 2 EL parameters of the PiG-based wLEDs with different mass ratios of phosphor to glass matrix ranging from 3 : 50 to 9 : 50

| Mass ratio | $x$ | $y$ | CCT (K) | $R_a$ | LE (lm W$^{-1}$) |
|---|---|---|---|---|---|
| 3 : 50 | 0.2439 | 0.1686 | — | — | — |
| 5 : 50 | 0.3137 | 0.2605 | 7487 | 73.9 | 78.6 |
| 7 : 50 | 0.3769 | 0.3386 | 3774 | 82.5 | 73.1 |
| 9 : 50 | 0.4036 | 0.3707 | 3364 | 76.6 | 68.4 |

Fig. 10 shows the EL spectra of the PiG (mass ratio = 7 : 50)-based wLED under different operating currents (50–300 mA). Upon increasing the operating current, the EL intensity of the fabricated wLED device enhanced. However, the corresponding coordinates shift from (0.3769, 0.3386) to (0.3629, 0.3101), the value of CCT increases from 3374 to 4186 K and the value of CRI also increases from 82.5 to 84.1. The variations of these values are slightly high, but within acceptable limits.[44] Such a

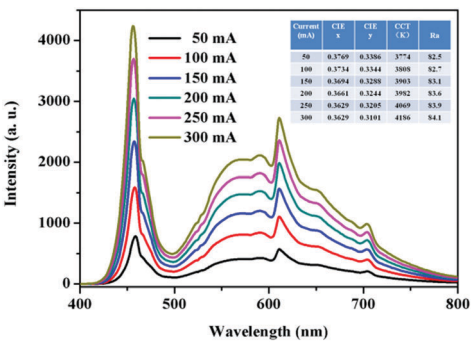


Fig. 10 EL spectra of the PiG (mass ratio = 7 : 50)-based wLED under different operating currents (50–300 mA). Corresponding parameters are shown in the inset.

situation can be attributed to the relatively reduced intensity of the emissive component of PiG along with the operating current as shown in Fig. S6 (ESI†). The overall QE of the PiG is slightly deficient and the PiG sample cannot be excited by the high-power blue chip adequately. The above problem observed in the PiG-based wLEDs will hopefully be solved through obtaining high QEs for the CaO:$Ce^{3+}$,$Li^{+}$,$F^{-}$ phosphor and the red-emitting host glass in the future. On the whole, the as-prepared PiG-based w-LEDs have acceptable color stability at various driving currents.

## 4. Conclusions

In summary, CaO:$Ce^{3+}$,$Li^{+}$,$F^{-}$ phosphors using $CeF_3$ and LiF as the cerium, lithium and fluorine sources were prepared through a high temperature solid-state reaction. The structure and luminescence as well as the stability of these materials were investigated in detail. As a result, the CaO:$Ce^{3+}$,$Li^{+}$,$F^{-}$ phosphors have more red components in their emission spectrum than YAG:$Ce^{3+}$. Notably, the critical doping concentration of $Ce^{3+}$ in the CaO:$Ce^{3+}$,$Li^{+}$,$F^{-}$ phosphors reached 0.06%, which is just a tenth of that of the $F^{-}$ undoped samples and accounts for the stronger luminescence. $F^{-}$ doping can effectively remove the impurity of $CeO_2$, which can influence the luminescence intensity of the phosphor. Furthermore, the representative COCLF-6 sample shows better QE of 66.4% and excellent thermal and chemical stability as compared to those of COCL-7. In order to acquire improved properties, the COCLF-6 phosphor was introduced into a red-emitting glass system with the composition of $SiO_2$–$Na_2CO_3$–$Al_2O_3$–CaO:$Eu^{3+}$ to fabricate various PiG substrates. The as-obtained PiG substrates with better performance show great potential for use in high-power wLEDs and the optimal PiG-based wLED has color coordinates of (0.3769, 0.3386), a CCT of 3774 K, a CRI of 82.5 and a LE of 73.1 when the mass ratio of phosphor to glass matrix is 7 : 50 in the PiG. Moreover, such PiG-based wLEDs also show acceptable color stability under different drive currents. Generally, CaO:$Ce^{3+}$,$Li^{+}$,$F^{-}$ can be expected to be an alternative yellow phosphor for blue-emitting excited warm wLEDs, particularly for high-power devices.

## Conflicts of interest

There are no conflicts to declare.

## Acknowledgements

The present study was supported by the National Natural Science Foundation of China (Grant No. 21671070), the Project for Construction of High-level University in Guangdong Province, the Teamwork Projects funded by the Guangdong Natural Science Foundation (Grant No. S2013030012842), the Guangzhou Science & Technology Project (No. 201704030086) and the Open Project Fund from Key Laboratory of Advanced of Materials of Yunnan Province (No. 2018KF01).

## Notes and references

1 J. Meyer and F. Tappe, *Adv. Opt. Mater.*, 2014, **3**, 424–430.
2 J. Cho, J. H. Park, J. K. Kim and E. F. Schubert, *Laser Photonics Rev.*, 2017, **11**, 1600147.
3 J. Li, J. Yan, D. Wen, W. U. Khan, J. Shi, M. Wu, Q. Su and P. A. Tanner, *J. Mater. Chem. C*, 2016, **4**, 8611–8623.
4 Z. Xia and A. Meijerink, *Chem. Soc. Rev.*, 2017, **46**, 275–299.
5 H. Chen, H. Lin, J. Xu, B. Wang, Z. Lin, J. Zhou and Y. Wang, *J. Mater. Chem. C*, 2015, **3**, 8080–8089.
6 J.-J. Shyu and C.-W. Yang, *Mater. Chem. Phys.*, 2017, **193**, 339–347.
7 Y. Tang, S. Zhou, X. Yi, S. Zhang, D. Hao and X. Shao, *J. Am. Ceram. Soc.*, 2017, **100**, 2590–2595.
8 Y. Wu, Z. Chi and T. He, *J. Mater. Sci.: Mater. Electron.*, 2017, **28**, 14591–14595.
9 K. Bartosiewicz, V. Babin, J. A. Mares, A. Beitlerova, Y. Zorenko, A. Iskaliyeva, V. Gorbenko, Z. Bryknar and M. Nikl, *J. Lumin.*, 2017, **188**, 60–66.
10 C.-e. Huang, X. Lu, M. Lu and Y. Huan, *Ceram. Int.*, 2017, **43**, 10624–10627.
11 S. M. Salman, S. N. Salama and H. A. Abo-Mosallam, *Ceram. Int.*, 2017, **43**, 9424–9430.
12 P.-L. Boey, G. P. Maniam and S. A. Hamid, *Chem. Eng. J.*, 2011, **168**, 15–22.
13 W. Lehmann, *J. Lumin.*, 1973, **6**, 455–470.
14 A. Yousif, R. E. Kroon, E. Coetsee, O. M. Ntwaeaborwa, H. A. A. Seed Ahmed and H. C. Swart, *Appl. Surf. Sci.*, 2015, **356**, 1064–1069.
15 D. Prakash and K. R. Nagabhushana, *Nucl. Instrum. Methods Phys. Res., Sect. B*, 2016, **379**, 136–140.
16 Y. Jin, Y. Hu, L. Chen, X. Wang, G. Ju, Z. Mou and F. Liang, *Opt. Commun.*, 2013, **311**, 266–269.
17 L. Feng, Z. Hao, X. Zhang, L. Zhang, G. Pan, Y. Luo, L. Zhang, H. Zhao and J. Zhang, *Dalton Trans.*, 2016, **45**, 1539–1545.
18 Q. Liu, H. Yin, T. Liu, C. Wang, R. Liu, W. Lü and H. You, *J. Lumin.*, 2016, **177**, 349–353.
19 Z. Hao, X. Zhang, Y. Luo, L. Zhang, H. Zhao and J. Zhang, *J. Lumin.*, 2013, **140**, 78–81.
20 Z. Hao, X. Zhang, X. Wang and J. Zhang, *Mater. Lett.*, 2012, **68**, 443–445.
21 D. Chen, W. Xiang, X. Liang, J. Zhong, H. Yu, M. Ding, H. Lu and Z. Ji, *J. Eur. Ceram. Soc.*, 2015, **35**, 859.
22 Y. K. Lee, J. S. Lee, J. Heo, W. B. Im and W. J. Chung, *Opt. Lett.*, 2012, **37**, 3276–3278.
23 R. Zhang, H. Lin, Y. Yu, D. Chen, J. Xu and Y. Wang, *Laser Photonics Rev.*, 2014, **8**, 158–164.
24 X. Zhang, J. Yu, J. Wang, C. Zhu, J. Zhang, R. Zou, B. Lei, Y. Liu and M. Wu, *ACS Appl. Mater. Interfaces*, 2015, **7**, 28122–28127.
25 J. Zhong, D. Chen, Y. Zhou, Z. Wan, M. Ding, W. Bai and Z. Jia, *Dalton Trans.*, 2016, **45**, 4762–4770.
26 F. Iqbal, S. Kim and H. Kim, *Opt. Mater.*, 2017, **72**, 323–329.
27 J. Zhong, W. Xu, Q. Chen, S. Yuan, Z. Ji and D. Chen, *Dalton Trans.*, 2017, **46**, 9959–9968.

28 X. Zhang, J. Yu, J. Wang, B. Lei, Y. Liu, Y. Cho, R.-J. Xie, H.-W. Zhang, Y. Li, Z. Tian, Y. Li and Q. Su, *ACS Photonics*, 2017, **4**, 986–995.
29 Q.-Q. Zhu, X. Xu, L. Wang, Z.-F. Tian, Y.-Z. Xu, N. Hirosaki and R.-J. Xie, *J. Alloys Compd.*, 2017, **702**, 193–198.
30 S. Yi, W. J. Chung and J. Heo, *J. Am. Ceram. Soc.*, 2017, **100**, 2378–2381.
31 H.-A. Park, Y. K. Lee, W. B. Im, J. Heo and W. J. Chung, *Opt. Mater.*, 2015, **41**, 67–70.
32 J. Deng, W. Li, H. Zhang, Y. Liu, B. Lei, H. Zhang, L. Liu, X. Bai, H. Luo, H. Liu, W.-R. Liu and J. Wang, *Adv. Opt. Mater.*, 2017, **5**, 1600910.
33 S.-P. Lee, C.-H. Huang, T.-S. Chan and T.-M. Chen, *ACS Appl. Mater. Interfaces*, 2014, 6, 7260–7267.
34 H. Li, R. Zhao, Y. Jia, W. Sun, J. Fu, L. Jiang, S. Zhang, R. Pang and C. Li, *ACS Appl. Mater. Interfaces*, 2014, **6**, 3163–3169.
35 Bruker AXS, *TOPAS V4.2: General profile and structure analysis software for powder diffraction data—User's Manual*, Bruker AXS, Karlsruhe, Germany, 2008.
36 W. Primak, H. Kaufman and R. Ward, *J. Am. Chem. Soc.*, 1948, **70**, 2043–2046.
37 H. E. Petch, *Acta Crystallogr.*, 1961, **14**, 950–957.
38 M. Yashima and S. Kobayashi, *Appl. Phys. Lett.*, 2004, **84**, 526–528.
39 Z. Wang, J. Zou, Y. Li, C. Zhang, M. Shi, B. Yang, H. Zhou, Y. Liu and N. Liu, *J. Mater. Sci.: Mater. Electron.*, 2017, **28**, 16633–16638.
40 X. Liu, F. Wu, S. Chen, M. Gu, H. Chen, B. Liu, S. Huang and J. Zhang, *J. Lumin.*, 2015, **161**, 422–425.
41 E. Song, J. Wang, S. Ye, X.-B. Yang, M. Peng, Q. Zhang and L. Wondraczek, *Adv. Opt. Mater.*, 2017, **5**, 1700070.
42 R.-J. Xie, N. Hirosaki, N. Kimura, K. Sakuma and M. Mitomo, *Appl. Phys. Lett.*, 2007, **90**, 191101–191103.
43 Y.-C. Wu, D.-Y. Wang, T.-M. Chen, C.-S. Lee, K.-J. Chen and H.-C. Kuo, *ACS Appl. Mater. Interfaces*, 2011, **3**, 3195–3199.
44 Y. H. Kim, P. Arunkumar and W. B. Im, *Ceram. Int.*, 2015, **41**, 5200–5204.

 